Human–Machine Cooperative Steering Control Considering Mitigating Human–Machine Conflict Based on Driver Trust

Zhuqing Shi, Hong Chen, *Senior Member, IEEE*, Ting Qu, and Shuyou Yu

***Abstract*—To reduce the impact of human–machine conflict on vehicle safety, this study proposes a novel human–machine cooperative steering control approach from the perspective of driver trust in the machine. The relationship between driver trust in the machine and driving skill is analyzed by the chi-square test method, and an online cooperative algorithm is designed using fuzzy control for different conditions, which assigns control authority based on driver trust under safe conditions and gives most of the authority to the machine to ensure safety under dangerous conditions. The machine is designed using model predictive control as an alternative controller parallel to the driver. To implement the proposed approach, a simulation platform that includes drivers and a test vehicle is established. Based on the driving data of human drivers collected in field tests, a two-point visual driver model is established to simulate steering behaviors and reflect physical workload. The parameters of the driver model are identified by a particle swarm optimization method to represent different drivers. The effectiveness of the approach, such as guaranteeing vehicle safety and reducing physical workload and human–machine conflict, is verified by simulations under typical conditions and obstacle avoidance conditions based on veDYNA vehicle dynamics software.**

***Index Terms*—Driver trust, human–machine conflict, human–machine cooperative control, model predictive control (MPC).**

I. Introduction

DURING the development of vehicle intelligence, human–machine cooperative control is an important stage before full automation [1], [2]. In this stage, the machine cooperates with a human driver in perception, decision-making, and action to share vehicle control tasks, reduce physical workload, and ensure vehicle safety [3]. However, many types of human–machine conflicts may occur during the interaction, such as different intentions and reverse action [4], which introduce great difficulties for vehicle intelligence [5], [6].

The study of mitigating human–machine conflict in cooperative control is necessary for ensuring vehicle safety and avoiding serious accidents. When a conflict suddenly occurs, human drivers are not capable of making immediate judgments and assigning control authority, which may cause deaths as reported in the news [7]. Judging which agent is correct and designing a corresponding control authority are two important issues worth discussing. Solutions to the issues have not been fixed in the form of policies and regulations, and they are still open-ended challenges.

One approach reserves the decision-making and control authority to the human driver, using sound, vision, and touch as reminders, such as lane departure warning [8] and forward collision warning [9]. In such systems, the human driver is supposed to be right all the time. Although research on such systems completely avoids human–machine conflicts in decision-making and action, they are incapable of taking over the vehicle to reduce any risk under driver nonresponse.

Another approach involves the design of explicit switching control and a dynamic designed cooperative strategy between the human driver and machine. In switching control, the control authority is explicitly changed by a physical mechanism in specific situations. Related research contains the judgment of appropriate switching time [10], arousing driver attention [11], and study of switching control methods [12]. This control avoids the conflict of actions between the human driver and machine, and only one agent is in the control loop at a time. However, a sudden takeover request from the machine will cause human drivers to be unaware of the situation. In that brief moment, it is difficult for a human driver to correctly judge whether the machine should take over and then operate the physical mechanism.

In contrast to switching control methods, a dynamic designed cooperative strategy cannot completely eliminate human–machine conflict because the human driver is always interacting with the machine in the control loop [4]. Two control frameworks for designing cooperative strategies include direct shared control

Manuscript received 23 July 2021; revised 12 March 2022 and 16 May 2022; accepted 13 June 2022. Date of publication 2 August 2022; date of current version 15 September 2022. This work was supported in part by the National Key R&D Program of China under Grant 2020AAA0108101, in part by the National Natural Science Foundation of China under Grant 61790564 and Grant U1964202, and in part by the Jilin Provincial Educational Foundation of China under Grant JJKH20211095KJ. This article was recommended by Associate Editor C. Wu. *(Corresponding author: Ting Qu)*

Zhuqing Shi and Shuyou Yu are with the Department of Control Science and Engineering, Jilin University, Changchun 130012, China, and also with State Key Laboratory of Automotive Simulation and Control, Jilin University, Changchun 130025, China (e-mail: shizq18@mails.jlu.edu.cn; shuyou@jlu.edu.cn).

Hong Chen is with the Department of Control Science and Engineering, Jilin University, Changchun 130012, China, and also with the College of Electronics and Information Engineering, Tongji University, Shanghai 200092, China (e-mail: chenhong2019@tongji.edu.cn).

Ting Qu is with the State Key Laboratory of Automotive Simulation and Control, Jilin University, Changchun 130025, China, and also with the Key Laboratory of Industrial Internet of Things and Networked Control, Chongqing University of Posts and Telecommunications, Chongqing 400065, China (e-mail: quting@jlu.edu.cn).

Color versions of one or more figures in this article are available at https://doi.org/10.1109/THMS.2022.3190683.

Digital Object Identifier 10.1109/THMS.2022.3190683

and indirect shared control [5]. Direct shared control enables both the human driver and automated machine to simultaneously exert actions on a control interface, of which the output directly controls the vehicle systems [5]. Such systems are usually haptic shared control (HSC), in which the human driver interacts with the machine directly through haptic feedback [13], [14]. The main drawback of HSC, which is also defined as coupled shared control, is the generation of torque conflicts between the driver and the automated system when they have different intentions [6]. To eliminate the conflict caused by increased steering torque between a human driver and a constant haptic support system, look-ahead controller adapting parameters are designed according to individual drivers [15]. A reference-free framework has been introduced to mitigate human–machine conflicts, in which time to collision and vehicle states were constrained to ensure vehicle safety [16].

For indirect shared control, the human driver and automated machine do not interact directly at a control interface [5]. The control inputs to the vehicle system are generated by mixing the control of a human driver (usually on the control interface) and an automated machine, which is the difference between direct shared control and indirect shared control. Indirect shared control claims to diminish human–machine conflicts, in which the machine does not interact directly with the human driver [17], [18]. A predictive model to capture driver adaption and trust in indirect shared control was proposed, which indicated that a driver's control effort is more sensitive to the trust level and that distrust would increase the driver steering effort [18]. Relevant research on the importance of human driver's trust in machines for vehicle safety has also been conducted [19], [20]. The framework of indirect shared control is taken for implementation in this study.

Instead of suddenly switching the driving authority between agents or changing the cooperative weight according to rules subjectively defined by researchers, this study proposes a human–machine cooperative control strategy from the perspective of driver trust in the machine. A cooperative algorithm is designed online for different conditions, assigning control authority based on driver attitude to the machine under safe conditions and giving most of the authority to the machine under dangerous conditions. The attitude of human drivers with different driving skills is analyzed using the chi-square test method, where the data are obtained through questionnaires collected from 67 randomly selected drivers. Based on the analysis, fuzzy control is used for the online design of the cooperative algorithm, which allocates the degree of cooperation according to driver attitude to the machine and vehicle safety. Using simulations under typical conditions and obstacle avoidance conditions, the effectiveness of mitigating human–machine conflict is verified.

To prevent excessive or insufficient intervention, the machine participates in vehicle control as an alternative controller parallel to the human driver [21], [22]. The machine is involved in the driving process only if it is needed to ensure vehicle safety. Since the mechanism of model predictive control (MPC) is similar to the driving process of a human driver and is capable of explicitly handling constraints, it is used to design the machine. To implement the proposed approach, a simulation platform including drivers and a test vehicle is established. Based on driving data of human drivers collected in field tests, a two-point visual driver model is established to simulate steering behaviors. The parameters of the driver model are identified using a particle swarm optimization (PSO) method to represent different drivers. The effectiveness of the approach, such as guaranteeing vehicle safety and reducing physical workload and human–machine conflict, is verified using simulations based on veDYNA vehicle dynamics software.

The article is organized as follows. First, Section II introduces the analysis of human driver's attitude and the strategy for mitigating human–machine conflict. Section III establishes the cooperative simulation platform. Then, Section IV provides the design of the automatic controller and online cooperative algorithm. In Section V, the effectiveness of the proposed algorithm is demonstrated through simulations under typical conditions and obstacle avoidance conditions. Finally, Section VI draws conclusions and discusses future work.

II. Human–Machine Cooperative Structure Based on Driver Trust

In the process of vehicle control, a machine performs better than human drivers in the aspect of fast and accurate execution, which is useful to help reduce physical workload and ensure vehicle safety. At the same time, the advantages of human drivers in environment perception and decision-making are irreplaceable by any existing vehicle intelligence machine technology. Although both advantages can be employed simultaneously in shared control, the possible conflict between the two controllers poses a new challenge to vehicle safety for shared control.

Conflicts between human drivers and machines may have many sources [4], such as different intention, information gathering, information processing, decision-making, and action implementation. Even if the reference trajectory is the same, different levels of driver need and trust in the machine can cause action conflict. In other words, if a human driver subjectively believes that they do not need or trust the assistance of the machine, the opposite action will occur, and vehicle safety may even be threatened.

To mitigate the action conflict, in this section, different degrees of human driver's need and trust in the machine based on driving skill classification and design of a corresponding human–machine cooperative control structure are studied. The reason for this classification is that human driver's driving skills are fixed and stable over a period of time, and such classification is also proven to be representative and reasonable in this section.

A. *Driver Attitude Toward the Machine*

To investigate human driver's need and trust in the machine, a questionnaire survey was conducted among 67 human drivers randomly recruited in the field test. The questionnaire is given by Table XI in the Appendix and involves the aspects of each human driver's actual years of driving, driving skill level, and willingness to be assisted by the machine under safe and dangerous conditions. Using the Mantel–Haenszel and chi-square test statistics method, the relationships among the three aspects are progressively determined as follows.

TABLE I
STATISTICAL RESULTS OF DRIVING SKILL LEVEL

Y \ L	1	2	3	Total
1	6	19	2	27
2	1	10	13	24
3	1	2	13	16
Total	8	31	28	67

Y: Years of driving, values 1, 2, and 3 represent the novice, experienced, and most experienced groups, respectively.
L: Driving skill level, values 1, 2, and 3 are poor, medium, and good levels, respectively.

TABLE II
WILLINGNESS UNDER SAFE CONDITIONS

S \ Y	1	2	3	Total
1	7 A	11 A,B	11 B	29
2	20 A	13 A,B	5 B	38
Total	27	24	16	67

Y: years of driving; *S*: willingness to be assisted under safe conditions, values 1 and 2 represent unwilling and willing, respectively.
Each subscript letter A or B denotes a subset of driver categories whose column proportions do not differ significantly from each other at the 0.05 level (confidence interval is 95%).

According to the years of driving, the 67 human drivers are divided into three groups: 1) a novice group, 2) experienced group, and most experienced group. In the novice group, years of driving are less than 4 with an average of 2.1 years. For the experienced group, years of driving are between 4 and 9 with an average of 5.6 years. In the most experienced group, the years of driving are all over 9 with an average of 18 years. Note that, the driving time and distance per day are also surveyed in the questionnaire, by which the total driving time and distance of each group are analyzed. Since the trends of total time and distance are consistent with actual years of driving, the years of driving are taken to represent actual driving experience.

First, the correlation between the years of driving and the driving skill level is analyzed by the Mantel–Haenszel chi-square test. It is assumed that the self-assessment is objective and can be used to represent the driving skill level. The self-assessment of driving skill is divided into good, medium and poor levels. The results are summarized in contingency Table I, in which the years of driving and driving skill level are regarded as two variables Y and L that both contain three values 1, 2, and 3. An initial hypothesis is developed as follows:

H0: Y and L are independent.

Then the Mantel-Haenszel test of linear association can be calculated as $\chi^2_{MH}= (W-1)r^2$, where $W = 67$ is the total, r is the Pearson correlation coefficient and defined as [23]

$$r = \frac{\operatorname{cov}(Y, L)}{\sqrt{S(Y)S(L)}} \tag{1}$$

where $\operatorname{cov}(Y, L)$ is the covariance of the variables Y and L, and the degrees of freedom are given by $df = 4$. Based on SPSS software, the two-sided asymptotic significance P1 of the Mantel-Haenszel chi-square test and the two-sided asymptotic significance P2 of the Pearson correlation coefficient are calculated. According to the results $\chi^2_{\mathrm{MH}}= 19.840$ and $\mathrm{P1} = 0.000 < 0.001$ (confidence interval 99.9%), hypothesis H0 should be rejected as there is a linear relationship between variables Y and L. Furthermore, according to the Pearson correlation coefficient results $r = 0.548$ and $\mathrm{P2} = 0.000 < 0.001$ (confidence interval 99.9%), there is a positive correlation between variables Y and L, which means that the driving skill level increases as years of driving increase. Based on this result, it is reasonable to classify driving skill according to years of driving.

Second, the relationship between the years of driving and driver need and trust in the machine is studied. The attitude of human drivers is shown in the contingency Table II, in which variable S represents the willingness to be assisted under safe conditions.

A null hypothesis for the relationship is developed as follows.

H0s: Under safe conditions, the driving years and willingness to be assisted are independent of each other.

To analyze the relationship between variables Y and S, Pearson's chi-square test is performed using data in contingency Table II as follows:

$$\chi^2_p = \sum_{ij} \frac{(f_{ij} - E_{ij})^2}{E_{ij}}, \quad E_{ij} = \frac{r_i c_j}{W} \tag{2}$$

where r_i and c_j are the ith row and jth column subtotal in the contingency Table II, respectively. f_{ij} is the observed value and E_{ij} is the expected count. The minimum expected count is $E_{\mathrm{min\_s}} = 6.93 > 5$, which satisfies the assumptions of using a chi-square test.

According to the chi-square test threshold table, the chi-square value corresponding to the significance level $\alpha = 0.05$ (confidence interval 95%) and the degrees of freedom $df = 2$ is the critical value $\chi^2 = 5.991$. Compared to this value, the result of Pearson's chi-square test under safe conditions is $\chi^2_{p\_s} = 7.604 > \chi^2$. The related two-sided asymptotic significance is $\mathrm{P3} = 0.022 < 0.05$. Therefore, hypothesis H0s should be rejected, as it means that at the significance level of $\alpha = 0.05$ (confidence interval 95%), there is a statistically significant difference in the assisted willingness of different groups under safe conditions.

Specifically, in contingency Table II, different subscript letters A and B show significant differences among groups of Y at the 0.05 significance level. There is a significant difference between groups 1 and 3. This again shows that drivers with different years of driving and driving skills have different willingness to be assisted under safe conditions. To further illustrate this relationship, Kendall's tau-b is used to analyze the correlation between variables Y and S. The correlation coefficient and significance results are $\tau_{bs} = -0.316 < 0$ and $\mathrm{P}_{bs} = 0.007 < 0.01$, respectively. Thus, variables Y and S have a negative correlation at the significance level of 0.01. In other words, the willingness of drivers to be assisted decreases with increasing years of driving.

The same analysis is also conducted under dangerous conditions using the data in contingency Table III. The null hypothesis H0d is that variables Y and D are independent. Pearson's chi-square is $\chi^2_{p\_\mathrm{d}} = 1.012 < \chi^2$ at the significance level $\alpha = 0.05$.

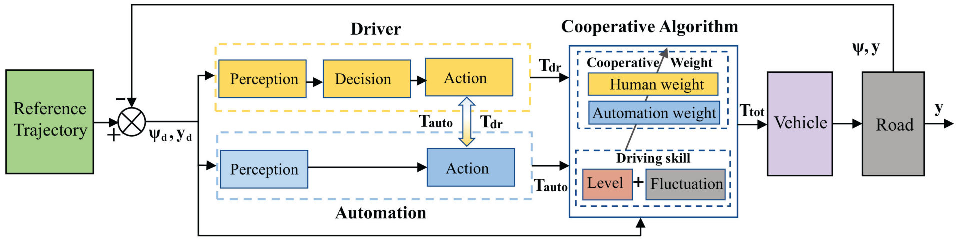

Fig. 1. Structure of the human–machine cooperative strategy.

TABLE III
WILLINGNESS UNDER DANGEROUS CONDITIONS

D \ Y	1	2	3	Total
1	4	6	4	14
2	23	18	12	53
Total	27	24	16	67

Y: years of driving; D: willingness to be assisted under dangerous conditions, values 1 and 2 represent unwilling and willing, respectively.

The two-sided asymptotic significance is $\mathrm{P4} = 0.603 > 0.05$. That is, the hypothesis should be accepted as there is no significant difference among the three groups of Y.

It can be seen from the above analysis that the human drivers' willingness to be assisted and driver's need and trust in the machine decrease with increasing years of driving and improvement of driving skill level. This feature is significant under safe conditions. The negative correlation between variables Y and S proves again that it is representative and reasonable to study different degrees of driver need and trust in the machine based on the classification of driving skill level. Furthermore, the corresponding human–machine cooperative control structure can be designed based on the analysis to mitigate human–machine conflict.

B. Control Structure to Mitigate Human–Machine Conflict

Based on different degrees of driver need and trust in the machine under safe conditions, the corresponding human–machine cooperative control structure is designed to mitigate human–machine conflict, as shown in Fig. 1. On the premise of vehicle safety, the cooperative algorithm is designed with a cooperative weight according to different driving skills. Since drivers with good driving skills are better at manipulation and environment comprehension, they have less need and trust in the machine, more driving authority is given to these drivers, and the automation should intervene as little as possible. On the contrary, drivers with poor driving skills are usually unable to act quickly and accurately, and they have more need and trust in the machine, so more driving authority is delegated to the automation.

As shown in Fig. 1, the automation is designed parallel to the human driver on the levels of perception, decision, and action. Since the human–machine conflict caused by human driver's attitude to the machine is considered, the automation collaborates with the human driver only on the action level in this study. Therefore, it is assumed that the reference trajectory of the automation and human driver is the same.

Under such an assumption, the automation and human drivers are consistent in their driving decisions. Aiming at tracking the reference trajectory, the human driver and automation exert torques T_{dr} and T_{auto} in parallel, respectively. According to the cooperative weight calculated using the cooperative algorithm and the MPC design, the total torque T_{tot} is applied to the vehicle system. Vehicle states and environmental information are measured by sensors and transmitted to the driver and automation.

Since subscript letters A and B in contingency Table II indicate that there is a significant difference between the novice group and the most experienced group at the 0.05 significance level, while there is no significant difference from the experienced group, human drivers' driving skills are divided into good and poor levels. The good level represents the most experienced drivers who can manipulate quickly and accurately, whereas the poor level describes the novice drivers who are unable to act accurately. These two levels are defined for driving skills in general conditions. However, the driving skill of an individual driver sometimes fluctuates due to unexpected reasons, such as fatigue, drunkenness, or bad mood. Thus, the cooperative algorithm is designed based on an online decision of driving skills, in which temporary fluctuation of driving skill can be considered. The details of this strategy are explained in the following sections.

III. SIMULATION PLATFORM INCLUDING DRIVERS

Considering the high cost of field tests and the complexity of repeatability, a human–machine cooperative control simulation platform is first established to implement the proposed method. The simulation platform introduces a driver model to represent the steering behavior of human drivers. Using the driving data of human drivers collected in the field test, the model parameters are identified according to drivers with different driving skills. Based on the veDYNA vehicle dynamics software, the vehicle is incorporated into the simulation platform.

A. Two-Point Visual Driver Model

To simulate steering behaviors and reflect the physical workload of human drivers, a two-point visual driver model is adopted. The output of the driver model is driver torque on the steering wheel that can better reflect the physical workload than the steering wheel angle [24], [25].

In the structure of the model depicted in Fig. 2, PI and P control are designed to keep tracking the road centerline and maintain stability. Based on the far-angle θ_f and near-angle θ_n

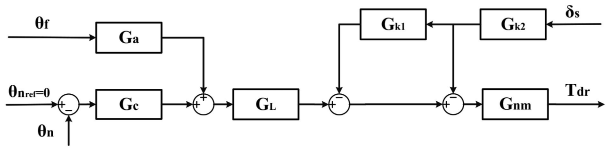

Fig. 2. Structure of the two-point visual driver model.

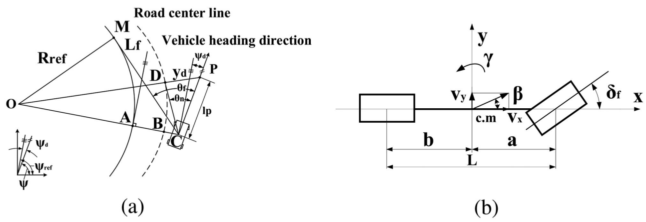

Fig. 3. Sketch of the vehicle. (a) Lateral motion. (b) 2-DOF vehicle model

shown in Fig. 3(a), the feedforward control and compensation control can be expressed as follows:

$$G_a = K_a, \qquad G_c = K_c \frac{T_L s + 1}{T_I s + 1} \tag{3}$$

where K_a is the proportional coefficient, K_c is the gain parameter, and T_L and T_I are the lead and lag time constants, respectively. The near-angle θ_n and far-angle θ_f previewed by drivers in the driving direction are approximated by

$$\theta_n \approx \frac{y_d}{l_p}, \qquad \theta_f \approx \frac{L_f}{R_{\text{ref}}} + \psi_d = L_f \rho_{\text{ref}} + \psi_d \tag{4}$$

where l_p and point P are the near distance and near point of previewing, respectively, and L_f and point M are the far distance and far point of previewing, respectively. The transfer functions for the driver response lag and muscular response lag are formulated as

$$G_L = e^{-\tau_p s} = \frac{1 - \frac{\tau_p}{2}s}{1 + \frac{\tau_p}{2}s}, \qquad G_{nm} = \frac{1}{T_N s + 1} \tag{5}$$

where τ_p is the processing delay time constant of driver brain and T_N is the lag time constant. The transfer functions G_{k1} and G_{k2} represent driver response to the feedback torque on the steering wheel and compensation of the resistance moment of the steering column, respectively. The transfer functions are

$$G_{k1} = K_d \frac{s}{s + \frac{1}{T_1}}, \qquad G_{k2} = K_G \frac{T_{K1} s + 1}{T_{K2} s + 1}. \tag{6}$$

B. Human Driver Driving Data Obtained From Field Tests

The established driver model can simulate the steering behavior of any driver for trajectory tracking. To reflect the driving skill level of individual drivers using the model, the driving data of different human drivers are collected and processed using field tests.

In the field tests, 6 drivers with representative driving skill levels are chosen from 67 drivers introduced in Section II-A. Drivers 1/2/3 of group 1 and drivers 4/5/6 of group 2 are selected from the novice and most experienced groups, respectively. Since human driver's need and trust in the machine are statistically different

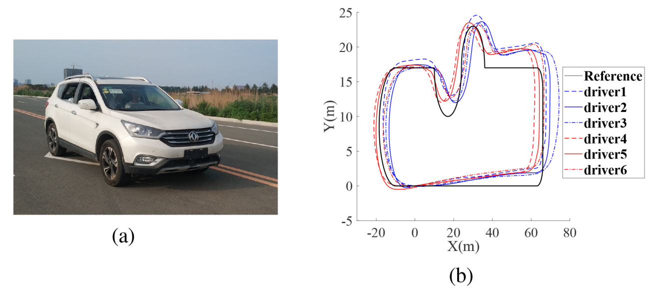

Fig. 4. Field test [(b): The black line is the reference trajectory; blue and red lines are trajectories of drivers with poor and good driving skills, respectively]. (a) Test vehicle. (b) Vehicle trajectories under custom coordinates.

under safe conditions, they are asked to control the vehicle and track the reference trajectory at a low speed of 10 km/h. The test vehicle, a DONGFENG AX7 as shown in Fig. 4(a), is equipped with an RT3002 inertial/GPS integrated navigation system to collect vehicle states including speed, position, steering wheel torque, steering wheel angle, and angular velocity. For data processing, Universal Transverse Mercator projection is used to convert latitude and longitude coordinates to custom coordinates. The results of vehicle trajectories are shown in Fig. 4(b).

In the vehicle trajectories shown in Fig. 4(b), the black line is the reference trajectory and the blue and red lines represent drivers with poor and good driving skills, respectively. It can be seen from the lines that the displacement deviation and angular deviation are less for drivers with good driving skills than for drivers with poor driving skills, which is consistent with the accurate control ability of drivers with good driving skills.

C. Driver Model Parameter Identification

Using the driver model and driving data obtained above, driver model parameters are identified to reflect different driving skill levels. PSO, which has the advantages of fast optimization and easy realization, is introduced. Given a reference trajectory, the minimum mean square deviation of the output of the driver model and the driver torque from the field data are defined as the following fitness function:

$$f(x) = \sqrt{\frac{1}{n} \sum\nolimits_{i=1}^{n} \left[\mathrm{T}_{di} - \bar{\mathrm{T}}_{di}\right]^2} \tag{7}$$

where T_{di} is the driver torque exerted on the steering wheel, $\bar{T}_{di}$ is the output of the driver model and $n = 80$ is the number of particles. The position vector x of particle i is defined as $x_i = (K_{ai}, K_{ci})$ to represent driving skill variation, where K_{ai} is the proportional coefficient and K_{ci} is the gain parameter. The remaining parameters in the driver model are considered constants as shown in Table IV. To enhance the global and local search capability to converge to the global optimal solution, the inertia factor and acceleration factor model with linear variation are adopted [26]. The velocity and position of each particle are updated as follows:

$$v_{id}^{\,t+1} = \omega v_{id}^{\,t} + c_1 r_1 (p_{id} - x_{id}^{\,t}) + c_2 r_2 (p_{gd} - x_{id}^{\,t}) \tag{8}$$

$$x_{id}^{\,t+1} = x_{id}^{\,t} + v_{id}^{\,t+1}, \quad i = 1, 2, \ldots, n, \quad d = 1, 2 \tag{9}$$

TABLE IV
DRIVER MODEL FIXED PARAMETERS

Parameters	Values	Parameters	Values
T_1	4.5	T_L	2.2
K_G	-0.85	T_I	0.2
T_{K1}	2.99	τ_p	0.08
T_{K2}	0.043	l_p	9
T_N	0.2	L_s	20

TABLE V
IDENTIFIED PARAMETERS OF THE DRIVER MODEL

Parameters \ Driver	Group 1			Group 2		
	1	2	3	4	5	6
K_a	0.03	0.15	0.02	0.51	0.69	0.73
K_c	0.71	0.93	0.76	1.12	1.24	1.17

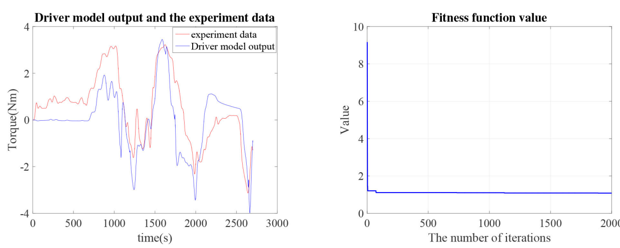

(a) (b)

Fig. 5. Identification results. (a) Driver model identification output and experimental data. (b) Fitness function value of PSO.

where t is the iteration number, $v_i = (v_{i1}, v_{i2})$ is the velocity vector, $p_i = (p_{i1}, p_{i2})$ and $p_g = (p_{g1}, p_{g2})$ are the best experience of the particle i and the group, respectively, r_1 and r_2 are random numbers following a random distribution in [0,1]. $v_{id} \in [-v_{\max}, v_{\max}]$ and $v_{\max} = x_{\max}$ are chosen for ensuring the rate of convergence and identification precision [27]. The number of iterations is $M = 2000$. c_1 and c_2 are learning factors. The inertia factor ω, which decreases linearly from $\omega_{\max}$ to $\omega_{\min}$, is adopted as in [28] and [29].

The model parameter identification results of the six drivers are shown in Table V. Taking driver 3 as an example, the results of the steering wheel torque and fitness function are shown in Fig. 5. As seen in Fig. 5(a), under the same road conditions, the identified steering wheel torque is consistent with that in the test, which reflects the steering behavior of the driver. As Fig. 5(b) shows, the small fitness function value indicates a high degree of fitting. Thus, the effectiveness of PSO for driver model parameter identification is verified. In addition, the performance of different driving skills reflected by different driver model parameters is described in Section V.

IV. DESIGN FOR AUTOMATION AND COOPERATIVE ALGORITHM

A. MPC for Automation

Since the mechanism of MPC is similar to the driving process of human drivers, including prediction, optimization, and execution, it is adopted as the automatic controller parallel to human drivers, as shown in Fig. 1.

A two-degree-of-freedom (2-DOF) vehicle model is adopted to express the lateral and yaw motion of the vehicle. A sketch of the 2-DOF vehicle model is shown in Fig. 3(b), and the dynamic equations with assumptions are expressed as [30], [31]

$$\dot{\beta} = -\frac{(C_f + C_r)}{mv_x}\beta + \left(\frac{(bC_r - aC_f)}{m{v_x}^2} - 1\right)\gamma + \frac{C_f}{mv_x}\delta_f \tag{10a}$$

$$\dot{\gamma} = \frac{(bC_r - aC_f)}{I_z}\beta - \frac{(a^2C_f + b^2C_r)}{I_z v_x}\gamma + \frac{aC_f}{I_z}\delta_f \tag{10b}$$

where m and β are the vehicle mass and the sideslip angle of the center of mass (c.m.), respectively, I_z and γ are the moment of inertia and the yaw rate about the yaw axis, respectively, v_x is the longitudinal velocity of the c.m. in the vehicle coordinate system, a and b are distances from the front and rear wheel axles to the c.m., respectively, C_f and C_r are the cornering stiffnesses of the front and rear tires, respectively, δ_f is the steering angle of the front wheel. A steering column model is established as [32]

$$J_s\dot{\omega}_s = -b_s\omega_s - T_{sw} + T_{\text{tot}} \tag{11}$$

$$\dot{\delta}_s = \omega_s \tag{12}$$

where T_{tot} is the total torque exerted on the steering wheel, ω_s is the steering wheel angle rate and $\delta_s = g_s \cdot \delta_f$ is the steering wheel angle, where g_s is the gear ratio. b_s and J_s are the friction coefficient and moment of inertia of the steering column, respectively. The wheel aligning torque on the steering system is

$$T_{sw} = \frac{K_s\alpha_f}{g_s} \tag{13}$$

where $K_s = -K_pC_f\eta_t$ is the aligning torque coefficient, η_t is the sum of the tire trailing distance and caster moment arm, and K_p is the steering system coefficient. The sideslip angle α_f is modeled in the linear region as

$$\alpha_f = \beta + \frac{l_f\gamma}{v_x} - \delta_f. \tag{14}$$

To describe the vehicle kinematics and trajectory in the inertia coordinate system, a road perception model is introduced [24]. In Fig. 3(a), C denotes the c.m. of the vehicle. It is assumed that the lookahead point P is observed by drivers along the vehicle heading direction and that the lookahead distance l_p is the length of CP. The vertical distance DP between P and the road centerline is defined as the lateral displacement deviation $y_d = y - y_{\text{ref}}$, in which y is the lateral displacement and y_{ref} is the reference along the road centerline. The reference curvature $\rho_{\text{ref}} = 1/R_{\text{ref}}$ is the curvature of the inner lane line, in which R_{ref} is the radius of curvature. The angle deviation ψ_d is the angle between the heading direction of the vehicle and the tangent direction of the road centerline, where $\psi_d = \psi_{\text{ref}} - \psi$, ψ is the yaw angle of the vehicle and ψ_{ref} is the reference of ψ along the tangent to the road centerline. Under the assumption that ψ_d is small, the deviation of the lateral displacement and angle can be described as

$$\begin{aligned}\dot{y}_d &= \dot{y} - \dot{y}_{\text{ref}} \\ &\approx v_x\beta + l_p\gamma - v_x\psi_d - v_x l_p \rho_{\text{ref}} \end{aligned} \tag{15}$$

$$\begin{aligned}\dot{\psi}_d &= \dot{\psi}_{\text{ref}} - \dot{\psi} \\ &= -\gamma + v_x\rho_{\text{ref}}. \end{aligned} \tag{16}$$

For the convenience of calculation, the vehicle dynamic equations and vehicle kinematic equations are rewritten in the discrete state-space equations as

$$x(k+1) = A_d x(k) + B_d u(k) + D_d w(k) \tag{17}$$

$$y = C_d x \tag{18}$$

where the sample time is $T_s = 0.01\ s$, $w = \rho_{\text{ref}}$ is the external input, the state vector and the output vector are $x = [\omega_s, \delta_s, \beta, \gamma, y_d, \psi_d]^T$ and $y = [y_d, \psi_d]^T$, respectively, and the control input $u = T_{\text{tot}}$ is defined as follows:

$$T_{\text{tot}} = \lambda T_{\text{auto}} + (1-\lambda) T_{\text{dr}} \tag{19}$$

where T_{dr} is the human driver's torque and T_{auto} is the MPC torque that needs to be designed, λ is the cooperative coefficient that is designed online using fuzzy control in the next section, and $\lambda = 1$ represents full driving automation. The system matrices are

$$A_d = \begin{bmatrix} -\frac{b_s}{J_s} & -\frac{K_p C_f \eta_t}{{g_s}^2 J_s} & \frac{K_p C_f \eta_t}{g_s J_s} & \frac{K_p C_f \eta_t a}{g_s J_s v_x} & 0 & 0 \\ 1 & 0 & 0 & 0 & 0 & 0 \\ 0 & \frac{C_f}{m v_x g_s} & -\frac{(C_f + C_r)}{m v_x} & \frac{(bC_r - aC_f)}{m {v_x}^2} - 1 & 0 & 0 \\ 0 & \frac{aC_f}{I_z g_s} & \frac{(bC_r - aC_f)}{I_z} & -\frac{(a^2 C_f + b^2 C_r)}{I_z v_x} & 0 & 0 \\ 0 & 0 & v_x & l_p & 0 & -v_x \\ 0 & 0 & 0 & -1 & 0 & 0 \end{bmatrix}$$

$$B_d = \begin{bmatrix} \frac{1}{J_s} & 0 & 0 & 0 & 0 & 0 \end{bmatrix}^{\mathrm{T}}, \quad C_d = \begin{bmatrix} 0 & 0 & 0 & 0 & 1 & 0 \\ 0 & 0 & 0 & 0 & 0 & 1 \end{bmatrix}$$

$$D_d = \begin{bmatrix} 0 & 0 & 0 & 0 & -v_x l_p & v_x \end{bmatrix}^{\mathrm{T}}.$$

The trajectory tracking problem can be described as the following optimization problem:

$$\begin{aligned} \min_{\Delta U(k)} J(x(k), u(k)) = \min_{\Delta U(k)} &||\Gamma_y (Y_{p,c}(k+1|k) \\ &- R(K+1))||^2 + ||\Gamma_u \Delta U(k)||^2 \\ \text{s.t.} \quad & x(k+1) = A_d x(k) + B_d u(k) + D_d w(k) \\ & Hx(k) \le G, \qquad i = 0, 1, \ldots, p \\ & \Delta u(k) = u(k) - u(k-1) \\ & u_{\min}(k+i) \le u(k+i) \le u_{\max}(k+i) \\ & \qquad i = 0, 1, \ldots, m-1 \\ & u(k+i) = 0, \quad i = m, m+1, \ldots, p-1 \end{aligned} \tag{20}$$

where $R(K+1) = [r(k+1), r(k+2), \ldots, r(k+p)]^T{}_{2p\times 1}$ is the reference vector. The vector of control increment $\Delta U(k) = [\Delta u(k), \Delta u(k+1), \ldots, \Delta u(k+m-1)]^T{}_{m\times 1}$ is the independent variable of the constrained optimization problem. The p steps control output $Y_{p,c}(k+1|k) = [y_c(k+1)|k, y_c(k+2)|k, \ldots, y_c(k+p)|k]^T{}_{2p\times 1}$ is predicted by the system model at time k. The control input constraint $u_{\max}(k) = -u_{\min}(k) = 8\ \mathrm{N}\cdot\mathrm{m}$ is introduced according to the actuator saturation of the steering system.

In (21), the state constraint $Hx(k) \le G$ is defined by a stable handling envelope to ensure vehicle stability, which is related to limits on the vehicle sideslip angle and yaw rate [33]. The limits show the maximum capacity of the given tires and subject to steady-state assumptions. The vehicle yaw rate constraint is

$$-\frac{g\mu}{v_x} \le \gamma \le \frac{g\mu}{v_x} \tag{21}$$

where g is the gravitational acceleration and μ is the road friction. The restriction of the vehicle sideslip angle is

$$-\alpha_p - \frac{b\gamma}{v_x} \le \beta \le \alpha_p - \frac{b\gamma}{v_x} \tag{22}$$

where $\alpha_p = \arctan(\frac{3mg\mu}{C_r} \cdot \frac{a}{a+b})$ is the slip angle related to the maximum lateral rear force. Then, the matrices H and G of the state constraint are

$$H = \begin{bmatrix} 0 & 0 & 0 & 1 & 0 & 0 \\ 0 & 0 & 0 & -1 & 0 & 0 \\ 0 & 0 & 1 & -\frac{b}{v_x} & 0 & 0 \\ 0 & 0 & -1 & -\frac{b}{v_x} & 0 & 0 \end{bmatrix}, G = \begin{bmatrix} \frac{g\mu}{v_x} \\ \frac{g\mu}{v_x} \\ \alpha_p \\ \alpha_p \end{bmatrix}. \tag{23}$$

B. Fuzzy Control for the Cooperative Algorithm

In this section, the cooperative algorithm is presented for deciding the cooperative coefficient in (19), which assigns control authority based on driver trust in the machine under safe conditions and provides most of the authority to the machine under dangerous conditions.

Fuzzy control, which works without mathematical models, is adopted for the online design of the cooperative coefficient. The reason for the online design is to prevent unexpected situations from affecting driving skills. As shown in Fig. 1, except for the basic driving skill level, the practical driving skill of a human driver is affected by sudden fluctuations. For example, an experienced driver may have poor driving skill due to fatigue or a bad mood. The impact of such fluctuations is considered by the online design of the fuzzy control.

In the fuzzy controller, the cooperative coefficient λ is the output and accounts for the cooperative weight of the machine. The absolute values of the lateral displacement deviation and angular deviation, i.e., $|y_d|$ and $|\psi_d|$, are chosen as inputs. Because the lateral displacement deviation y_d and angular deviation ψ_d between the vehicle trajectory and the reference trajectory are components of the inputs to the two-point visual driver model in (4), they reflect the driving skill of each driver in terms of tracking accuracy. Since the signs of variables y_d and ψ_d only indicate opposite directions, the absolute values $|y_d|$ and $|\psi_d|$ are used instead.

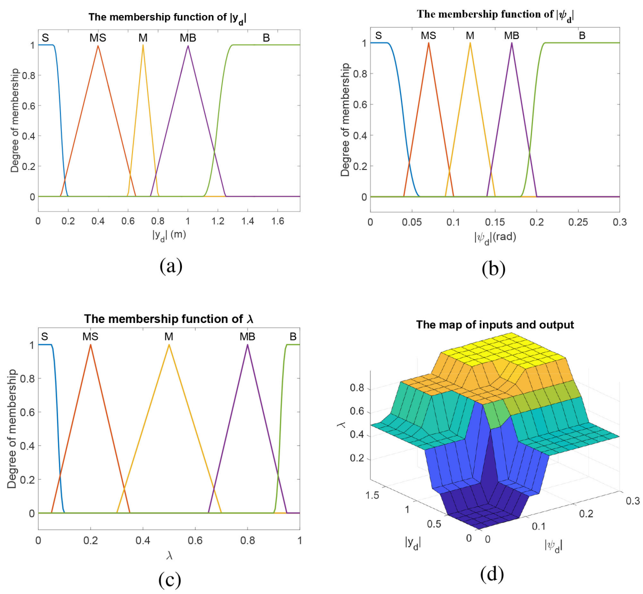

Fig. 6. Membership function and map in the fuzzy controller. (a) Membership function of $|y_d|$. (b) Membership function of $|\psi_d|$. (c) Membership function of λ. (d) Map of $|y_d|$, $|\psi_d|$, and λ.

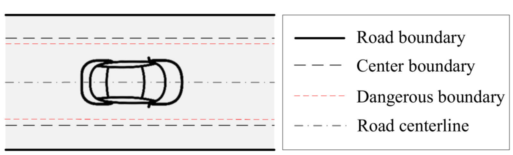

Fig. 7. Sketch of the lane diagram.

The membership functions of $|y_d|$, $|\psi_d|$, and λ are shown in Fig. 6(a)–(c) and are composed of Z-type, triangle, and S-type functions, which are divided into five sets, i.e., S, MS, M, MB, and B. The map of the relationships among $|y_d|$, $|\psi_d|$, and λ is shown in Fig. 6(d). The ranges of $|y_d|$, $|\psi_d|$, and λ are [0, 1.75] m, [0, 0.3] rad, and [0, 1], respectively. For $|y_d|$ and $|\psi_d|$, the specific values of the five sets are determined by the lane width and magnitude of tracking deviations.

In Fig. 6(a), the subsets from S to B correspond to increasing lateral displacement deviation. As shown in Fig. 7, the maximum value of $|y_d|$ is the half-width of the standard one-way lane, which corresponds to the road boundary with a solid black line, i.e., $L_w/2 = 1.75$ m. Since the vehicle width in the veDYNA software is $l_w = 1.644$ m, the distance deviation between the vehicle centerline and road boundary should be limited within $\text{Width}_c = (L_w - l_w)/2 = 0.928$ m, which is defined as the center boundary shown by the dashed black line in Fig. 7. An approximate value $\text{Width}_c \approx 1$ m is designed as the middle value of subset MB; when the value is greater than this middle value, it indicates that a large lateral displacement deviation belongs to MB or B.

Dangerous conditions are defined when the vehicle's c.m. is outside the dangerous boundary with $0.9 \cdot \text{Width}_c \approx 0.8$ m (presented by the dashed red line in Fig. 7). When the vehicle centerline is outside the dangerous boundary, the coefficient is selected as $\lambda = 0.9$, i.e., the machine has most of the control authority. To minimize interference with the driver, $|y_d| < 0.2 \cdot \text{Width}_c \approx 0.2$ m is considered to be no deviation, which is the max value of subset S.

In Fig. 6(b), the subsets from S to B correspond to increasing absolute values of the angular deviation $|\psi_d|$. In the interval [0, 0.3] rad of $|\psi_d|$, the intervals of the three subsets MS, M, and MB are evenly distributed and fuzzified by triangle functions. In Fig. 6(c), the subsets from S to B are distributed within the interval [0,1]. The cooperative coefficient $\lambda = 0.5$ corresponds to the middle value of subset M, which represents half driver control and half machine control. The other four subsets are symmetrically distributed about the middle value. By defuzzification of the gravity method, the value of λ is used for the MPC design.

The fuzzy rules are designed so that the value of λ increases as $|y_d|$ and $|\psi_d|$ increase, as shown in Table VI. Larger values of $|y_d|$ and $|\psi_d|$ imply that the driver has poorer driving skills in terms of tracking accuracy and higher need and trust in the machine, so a larger value of λ is designed to increase the control authority of the machine. The larger the value of λ is, the lower the control authority of the driver. Conversely, drivers with good driving skills correspond to smaller tracking deviations $|y_d|$ and $|\psi_d|$, and they require a smaller value of λ and greater control authority. This is in line with the discussion in Section II that human drivers' inclinations to need and trust the machine decrease with the improvement of driving skills.

TABLE VI
FUZZY RULES OF λ

$|\psi_d|$ \ $|y_d|$	S	MS	M	MB	B
S	S	S	MS	M	M
MS	S	S	MS	M	MB
M	MS	MS	M	MB	MB
MB	M	M	M	MB	B
B	M	M	MB	B	B

TABLE VII
VEHICLE PARAMETERS

Parameters	Values	Units	Parameters	Values	Units
m	1296	kg	C_f	35000·2	N/rad
I_z	1750	kg·m^2	C_r	35000·2	N/rad
l_f	1.25	m	g_s	20.4956	(-)
l_r	1.32	m	J_s	0.06	kg·m^2
b_s	0.1	N.ms/rad	K_p	0.024	(-)
ηt	0.25	m	l_w	1.644	m

V. Effectiveness of the Proposed Human–Machine Control Strategy

In this section, tests under typical and obstacle avoidance conditions are discussed to illustrate the effectiveness of the proposed approach in both normal and challenging scenarios. The parameters of the vehicle are listed in Table VII.

A. Tests Under Typical Conditions

In this section, simulation results are presented for the steady-state circular condition and double lane change (DLC)

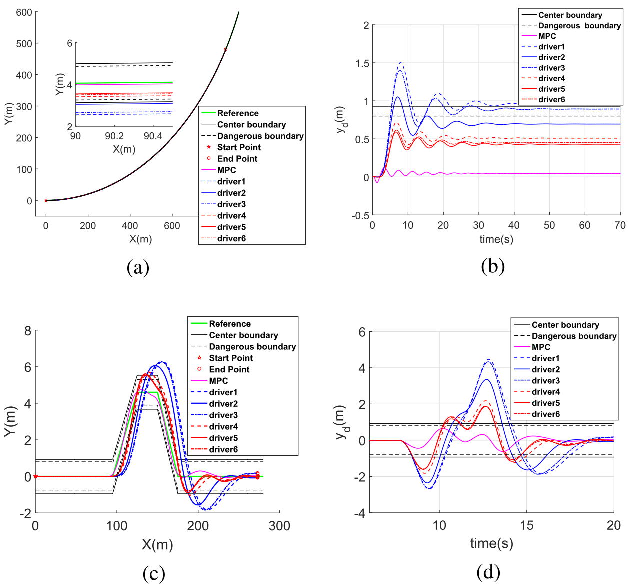

Fig. 8. Tracking results. (a) Vehicle trajectory under the circular condition. (b) Lateral displacement deviation under the circular condition. (c) Vehicle trajectory under the DLC condition. (d) Lateral displacement deviation under the DLC condition.

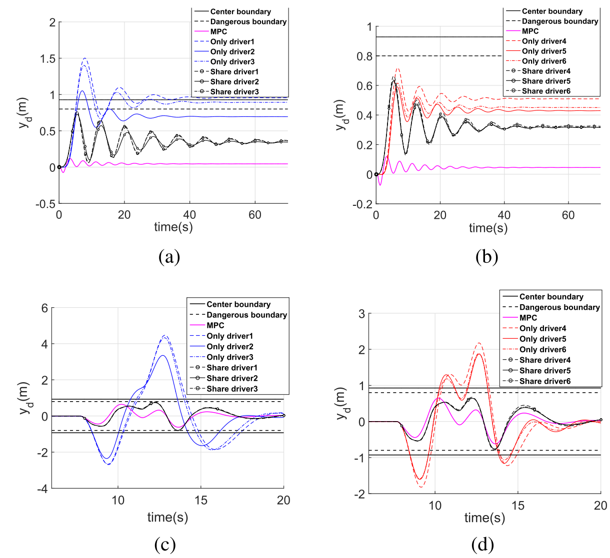

Fig. 9. Lateral displacement deviation of the cooperative algorithm. (a) Poor driving skill under the circular condition. (b) Good driving skill under the circular condition. (c) Poor driving skill under the DLC condition. (d) Good driving skill under the DLC condition.

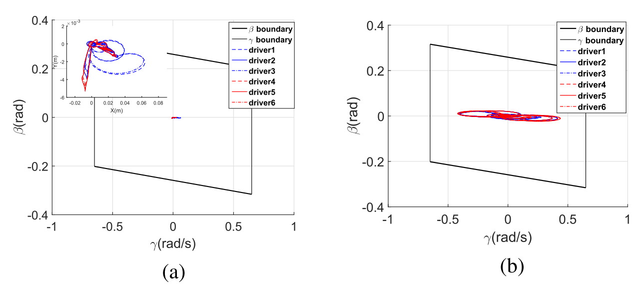

Fig. 10. Yaw rate and sideslip angle. (a) Under the circular condition. (b) Under the DLC condition.

condition, which are considered to be representative of typical conditions. The radius of the reference circular trajectory is $R_{\text{ref}} = 1000$ m. The DLC condition is designed according to ISO/TR3888 standard. The longitudinal speed of the vehicle is a constant $v_x = 54$ km/h.

1) Performance of a Single Agent: The test of a single agent is first conducted based on the simulation platform. Either the driver or automation controls the vehicle to track the reference trajectory under two conditions. The vehicle trajectories and deviations are shown in Fig. 8, in which blue lines and red lines represent drivers 1/2/3 of group 1 and drivers 4/5/6 of group 2, respectively, the magenta line represents the MPC, and the solid and dashed black lines are the center boundary and dangerous boundary, respectively.

In the MPC, the control horizon and the prediction horizon are $m = 5$ and $p = 20$, respectively, and the weighting matrices are $\Gamma_y = 50 \times \mathbf{I}_{2p\times 2p}$ and $\Gamma_u = 0.1 \times \mathbf{I}_{m\times m}$. As shown in Fig. 8, the MPC performs the smallest tracking deviation and has the best tracking accuracy. Compared to drivers with poor driving skills, drivers with good driving skills have smaller tracking deviation and higher tracking accuracy. Such a difference in tracking performance is caused by the different parameters of the driver model, which are identified based on the driving data of the field tests.

As seen in Fig. 8, the lateral displacement deviations of drivers sometimes deviate beyond the centerline boundary. Vehicle safety cannot be guaranteed by human drivers under such circumstances, so it is necessary to design a human–machine cooperative control strategy for assistance. In addition, while the MPC has the highest tracking accuracy, the reason for designing a novel human–machine cooperative strategy rather than using a constant cooperative weight is explained in detail in the next section.

2) Superiority of the Novel Cooperative Algorithm: Based on the proposed simulation platform and cooperative algorithm, parallel human–machine cooperative steering control is carried out under the steady-state circular condition and the DLC condition. The control horizon, prediction horizon, and weighting matrices of the MPC are defined as in the previous section. The simulation results are shown in Figs. 9–14.

Based on the results, the effectiveness of the proposed method from the following aspects is illustrated:

1) help human drivers ensure vehicle safety;
2) reduce physical workload of human drivers;
3) mitigate human–machine conflict by considering driver attitude to the machine.

In contrast, the simulation results of any single agent are also plotted in Figs. 9–14, in which the legends are the same as before. The center boundary and dangerous boundary are represented by the solid and dashed black lines, respectively. In addition, the black lines with circles represent the results of the human–machine cooperative control.

With regard to the first aspect, the vehicle lateral displacement deviations and vehicle γ–β phase plane plots are shown in Figs. 9 and 10, respectively, which explain the effectiveness of

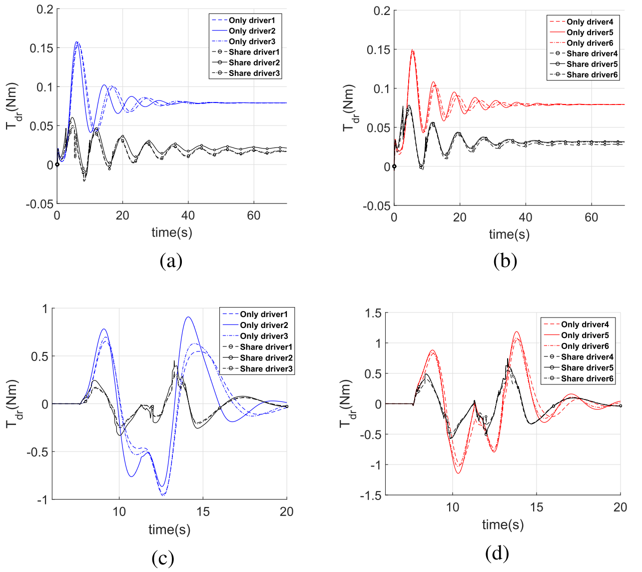

Fig. 11. Driver torque of the cooperative algorithm. (a) Poor driving skill under the circular condition. (b) Good driving skill under the circular condition. (c) Poor driving skill under the DLC condition. (d) Good driving skill under the DLC condition.

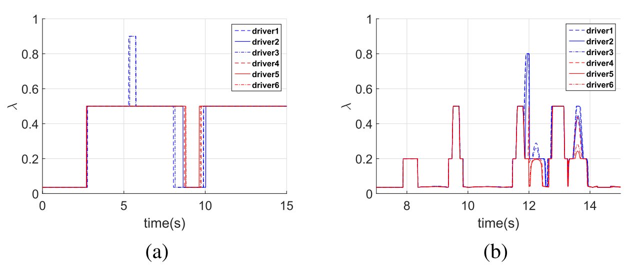

Fig. 12. Cooperative coefficient. (a) Under the circular condition. (b) Under the DLC condition.

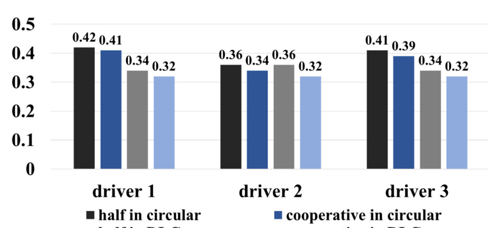

Fig. 13. RMS of the conflict rate of drivers with poor driving skill.

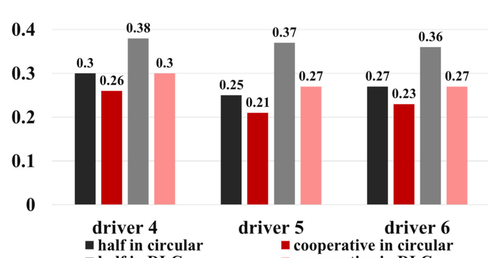

Fig. 14. RMS of the conflict rate of drivers with good driving skill.

TABLE VIII
RMS of the Driver Torque for the Circular Condition

Driver / $T_{\mathrm{dr\_rms}}$	Group					
	1			2		
	1	2	3	4	5	6
Without (N.m)	0.082	0.081	0.082	0.08	0.080	0.080
With (N.m)	0.019	0.025	0.020	0.031	0.035	0.034
Reduction (%)	76.8	69.1	75.6	61.3	56.3	57.5

Without/With: rms of the driver torque without/with cooperative control.
Reduction: Percentage reduction with cooperation compared to no cooperation.

TABLE IX
RMS of the Driver Torque for the DLC Condition

Driver / $T_{\mathrm{dr\_rms}}$	Group					
	1			2		
	1	2	3	4	5	6
Without (N.m)	0.33	0.38	0.35	0.38	0.41	0.39
With (N.m)	0.09	0.12	0.09	0.18	0.21	0.20
Reduction (%)	72.7	68.4	74.3	52.6	48.8	48.7

Without/With: rms of the driver torque without/with cooperative control.
Reduction: Percentage reduction with cooperation compared to no cooperation.

the proposed method in ensuring vehicle safety. As shown in Fig. 9, using the cooperative algorithm, vehicles are controlled with smaller lateral deviations. The designed cooperative control method ensures that the vehicle stays within the centerline boundary and dangerous boundary under both conditions. The relationship between the vehicle yaw rate and sideslip is shown in Fig. 10, and the solid black lines are the constraints defined in the MPC. Here, β and γ are all inside the constraints. Vehicle safety and stability, which are the most important requirements in cooperative control, are guaranteed by the proposed approach.

To illustrate the second aspect, driver torques under two conditions are shown in Fig. 11. The reduction in the physical workload is evaluated by the root mean square (rms) of the torque [34], which is defined as

$$T_{\mathrm{dr\_rms}} = \sqrt{\frac{1}{N}\sum\nolimits_{i=1}^{N} T_{\mathrm{dr}}(i)^2} \tag{24}$$

where N is the total sampling time. The results of $T_{\mathrm{dr\_rms}}$ controlled with cooperation and without cooperation are listed in Tables VIII and IX. As the percentages of the reduction in torque shown in Tables VIII and IX, the driver torque is significantly reduced in human–machine cooperative control compared to the case where the human driver is driving alone. This shows that the proposed algorithm can reduce physical workload on the human drivers.

In addition, as the cooperative coefficient shown in Fig. 12, drivers with good driving skills have smaller cooperative coefficients than those with poor driving skills. This means that in cooperative control, drivers with good driving skills have higher driving authority than those with poor driving skills. The result is consistent with the statistical analysis in Section II-A that drivers with good driving skills have less need and trust in the machine. It can be seen that the cooperative algorithm is designed according to human driver's attitude to the machine.

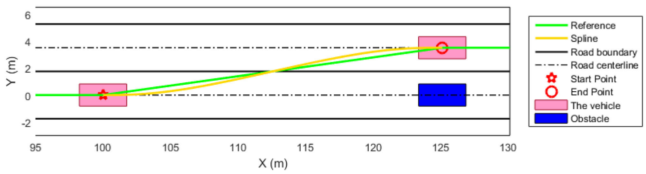

Fig. 15. Sketch of the LC.

Finally, the effectiveness of the proposed method to mitigate human–machine conflict in cooperative control is explained in Figs. 12–14.

The conflict rate and its rms value are defined to express the degree of human–machine conflict as follows:

$$\mathrm{Con} = \left| \frac{y_{\text{driver}} - y_{\text{co}}}{\max\left(y_{\text{driver}}\right)} \right| \tag{25}$$

$$\mathrm{Con}_{\text{rms}} = \sqrt{\frac{1}{N}\sum_{i=1}^{N} \mathrm{Con}(i)^2} \tag{26}$$

where y_{driver} and y_{co} represent the lateral displacement of steering control by the human driver and cooperative control, respectively. Here, a constant cooperative coefficient $\lambda = 0.5$ is introduced as the comparison to demonstrate the effectiveness of the proposed cooperative algorithm. The results of the rms value $\mathrm{Con}_{\text{rms}}$ of drivers with poor driving skill and good driving skill are shown in Figs. 13 and 14, respectively. As shown in the figures, the rms values are smaller for cooperative control than for a constant cooperative coefficient $\lambda = 0.5$ without considering driver attitude. This means that the novel cooperative algorithm designed according to human driver's attitude can effectively reduce human–machine conflict.

B. Tests Under Obstacle Avoidance Condition

In addition to the trajectory tracking results under typical conditions, the more challenging and practical scenario of obstacle avoidance is carried out to illustrate the effectiveness of the proposed method.

1) Path Planning for Obstacle Avoidance: The path planning of a lane change (LC) is adopted to avoid collisions caused by the sudden braking of the vehicle in front or the emergence of a fixed object. Assuming that there is no obstacle in the left lane, the vehicle is controlled to the left lane to avoid the near obstacle (vehicle or object) in the current lane. As shown in Fig. 15, the pink square and the blue square represent the vehicle to be controlled and the approaching obstacle, respectively, and the red pentagram and circle are the start point and end point of the LC, respectively.

In Fig. 15, the lateral distance of the LC is $S_{\text{LC}} = L_w = 3.5$ m, which is from the centerline of the current lane to that of the left lane. Assuming the lateral velocity and acceleration of the vehicle at the start and the end of the LC are zero, the shortest possible time of the LC should satisfy

$$t_{\text{LC}} = (2S_{\text{LC}}/a_y)^{\frac{1}{2}} > (2S_{\text{LC}}/0.4\,g)^{\frac{1}{2}} \approx 1.336\,\text{s} \tag{27}$$

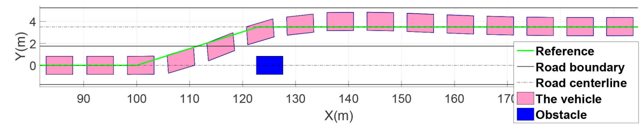

Fig. 16. Vehicle trajectory of the LC.

where the lateral acceleration $a_y < 0.4\,g$ ($g = 9.81\ \text{m/s}^2$) is the assumption of the 2-DOF vehicle model for lateral stability [30]. Therefore, $t_{\text{LC}} = 1.34$ s is chosen as the time of the LC considering lateral stability.

During the LC, the longitudinal speed and longitudinal acceleration of the vehicle are $v_x = 15$ m/s and $a_x = 0\ \text{m/s}^2$, respectively, and the longitudinal speed of obstacle is reduced to $0 \le v_{\text{ob}} < v_x$, i.e., the deviation of longitudinal speed satisfies $0 < \Delta v = v_x - v_{\text{ob}} \le 15$ m/s. The minimum longitudinal distance, which the collision can be avoided by the LC with lateral stability and without braking, is

$$\Delta x_{\min} = \Delta v \times t_{\text{LC}} = 20.1\,\text{m}. \tag{28}$$

Considering that the length of the vehicle or the obstacle is 5 m, the distance between the c.m. of the vehicle and the c.m. of the obstacle is set to $\Delta x = 25.1$ m at the start of the LC, as shown by the longitudinal distance between the red pentagram and the blue square in Fig. 15.

For trajectory planning, the reference trajectory is obtained by the five-spline curve-fitting method as shown by the yellow curve in Fig. 15. The fitting equations are

$$X_{\text{LC}}(t) = 6.94t^5 - 23.26t^4 + 20.78t^3 + 15t + 100 \tag{29a}$$

$$Y_{\text{LC}}(t) = 4.86t^5 - 16.28t^4 + 14.55t^3 \tag{29b}$$

where $X_{\text{LC}}(t)$ and $Y_{\text{LC}}(t)$ are the longitudinal position and lateral position at time t, respectively.

As seen in Fig. 15, the green line connecting the start and end points is very close to the yellow curve. Therefore, to maintain consistency with the trajectory planning of the DLC condition, the simplified green line is chosen as the reference trajectory for the LC.

2) Performance of the Cooperative Algorithm: By tracking the planned reference trajectory, the proposed approach is demonstrated to work well in challenging obstacle avoidance conditions. The simulation results are shown in Figs. 16–22, where the black lines with circles represent the results by the cooperative algorithm, the magenta lines denote the pure MPC, and the red lines and the blue lines represent drivers with good driving skills and drivers with poor driving skills, respectively.

The vehicle trajectories controlled by the six drivers with the cooperative algorithm are shown in Fig. 16, where the pink squares and the blue square represent the vehicle and the fixed obstacle, respectively, and the green line is the reference trajectory. As seen in Fig. 16, the vehicle starts to change the lane at $X = 100$ m and successfully avoids the fixed obstacle. Since the vehicle being controlled can avoid a fixed obstacle whose velocity is $v_{\text{ob}} = 0$ m/s, it can certainly avoid the front vehicle that suddenly brakes to a velocity of $0 \le v_{\text{ob}} < 15$ m/s.

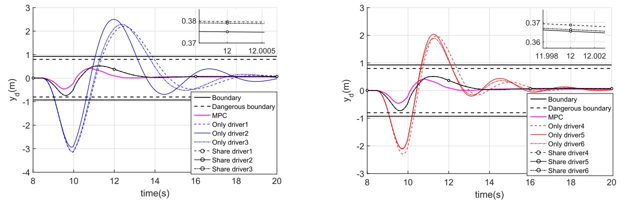

(a) (b)

Fig. 17. Lateral displacement deviation. (a) Poor driving skill. (b) Good driving skill.

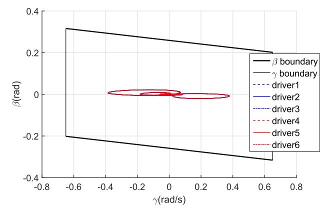

Fig. 18. Yaw rate and sideslip angle.

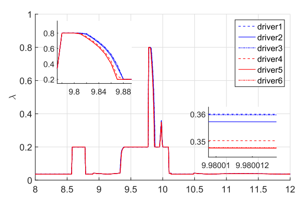

Fig. 19. Cooperative coefficient.

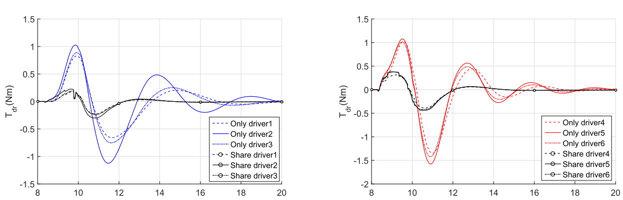

(a) (b)

Fig. 20. Driver torque. (a) Poor driving skill. (b) Good driving skill.

The lateral displacement deviations are largely reduced by the cooperation of the designed algorithm, which ensures vehicle safety. The deviations controlled only by drivers, by the pure MPC, and by the designed cooperative algorithm are shown in Fig. 17. The deviations by the designed cooperative algorithm are lower than 0.8 m, i.e., within the dangerous boundary shown by the dashed black lines. Furthermore, the values of β and γ are all within the boundaries shown by the solid black lines in Fig. 18, which means that the lateral stability of the vehicle is also guaranteed.

As shown by the driver torque in Fig. 19, the cooperative coefficients are designed smaller for drivers with good driving skills than those for drivers with poor driving skills. The small difference in the cooperation coefficient is because the tracking deviations of the pure driver controls are all large in such conditions.

TABLE X
RMS OF THE DRIVER TORQUE FOR OBSTACLE AVOIDANCE

Driver / $T_{\text{dr\_rms}}$	Group					
	1			2		
	1	2	3	4	5	6
Without (N.m)	0.25	0.36	0.27	0.36	0.41	0.37
With (N.m)	0.06	0.08	0.06	0.11	0.13	0.13
Reduction (%)	76.0	77.8	77.8	69.4	68.3	64.9

Without/With: rms of the driver torque without/with cooperative control.
Reduction: Percentage reduction with cooperation compared to no cooperation.

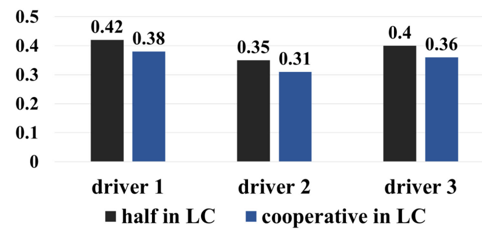

Fig. 21. RMS of the conflict rate of drivers with poor driving skill.

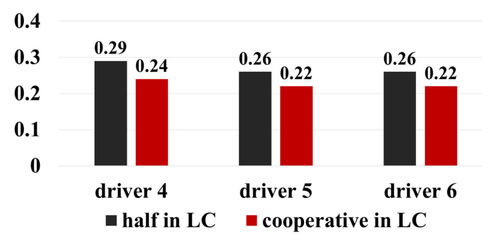

Fig. 22. RMS of the conflict rate of drivers with good driving skill.

As shown in Fig. 20, the physical workload of human drivers can be largely reduced by the proposed algorithm. To evaluate the reduction in torque, the rms of the torque corresponding to each driver is listed in Table X. The percentages of the reduction in driver torques by the cooperation are all over 60%, which means that the proposed method is able to reduce the physical workload of drivers.

In terms of human–machine conflict mitigation, the rms value of the conflict rate is compared with that of the fixed cooperative coefficient $\lambda = 0.5$, and the results are shown in Fig. 21 and Fig. 22. The black bars represent the results of $\lambda = 0.5$, whereas the blue and red bars denote the results of drivers with poor driving skill and good driving skill, respectively. It can be seen that the conflict rates of the proposed cooperative algorithm are smaller than those of the fixed coefficient that does not consider driver attitude.

VI. Conclusion

This research designs a human–machine cooperative strategy to mitigate human–machine conflict by considering human driver's trust in the machine. Using a statistical analysis method, it is determined that human driver's trust in the machine decreases with the improvement of the driving skill level under safe conditions. The machine, which is designed using an MPC, is parallel to the human driver. Fuzzy control is used to design the online cooperative algorithm for different conditions, which assigns control authority by driver trust under safe conditions and gives little authority to drivers to ensure safety under dangerous conditions. Using the simulation platform containing the developed driver model, the effectiveness of the proposed approach in ensuring vehicle safety, reducing physical workload, and mitigating human–machine conflict is illustrated through simulations under typical conditions and obstacle avoidance conditions. Future work includes introducing real human drivers and conducting driver-in-the-loop experiments to test the performance of the proposed approach. Due to the restrictions of safety regulations and the lack of hardware equipment, such as a driving simulator, this study uses the trained driver model as a virtual human driver for testing. Although driver models can be used to represent human drivers in shared control, the introduction of real human drivers for driver-in-the-loop experiments will enable further validation of the performance of this study.

Appendix
The Questionnaire

TABLE XI
Driver Trust in the Machine

Basic Information	
Name	
Gender	
Occupation	
Actual years of driving	
Time/distance of driving per day	
Questions	
Self-assessment of driving skill	(poor/medium/good)
Are you willing to be assisted under safe conditions	(Willing/Unwilling)
Are you willing to be assisted under dangerous conditions	(Willing/Unwilling)

References

[1] Y. Hu, T. Qu, J. Liu, Z. Shi, and B. Zhu, "Human-machine cooperative control of intelligent vehicle: Recent developments and future perspectives," *Acta Autom. Sin.*, vol. 45, no. 7, pp. 1261–1280, Jul. 2019.

[2] SAE, "On-road automated vehicle standards committee. taxonomy and definitions for terms related to on-road motor vehicle automated driving systems," *SAE Standard J.*, vol. 3016, pp. 1–16, 2014.

[3] H. Chen, L. Guo, and N. Bian, "On automobile intelligentization and key technologies," *Sci. Technol. Rev.*, vol. 35, no. 11, pp. 52–59, Nov. 2017.

[4] M. Itoh, F. Flemisch, and D. Abbink, "A hierarchical framework to analyze control conflicts between human and machine," *IFAC PapersOnLine*, vol. 49, no. 19, pp. 96–101, 2016.

[5] W. S. Wang et al., "Decision-making in driver-automation shared control: A review and perspectives," *IEEE-CAA J. Autom. Sin.*, vol. 7, no. 5, pp. 1289–1307, Sep. 2020.

[6] M. Marcano, S. Diaz, J. Perez, and E. Irigoyen, "A review of shared control for automated vehicles: Theory and applications," *IEEE Trans. Human-Mach. Syst.*, vol. 50, no. 6, pp. 475–491, Dec. 2020.

[7] Global Times, "Tesla Crashes in S. China at 158 km/h, sparks fresh worry over brake issues," May 2021. [Online]. Available: https://www.globaltimes.cn/page/202105/1222977.shtml

[8] J. Son, H. Yoo, S. Kim, and K. Sohn, "Real-time illumination invariant lane detection for lane departure warning system," *Expert Syst. Appl.*, vol. 42, no. 4, pp. 1816–1824, Mar. 2015.

[9] K. D. Kusano and H. C. Gabler, "Safety benefits of forward collision warning, brake assist, and autonomous braking systems in rear-end collisions," *IEEE Trans. Intell. Transp. Syst.*, vol. 13, no. 4, pp. 1546–1555, Dec. 2012.

[10] J. Nilsson, P. Falcone, and J. Vinter, "Safe transitions from automated to manual driving using driver controllability estimation," *IEEE Trans. Intell. Transp. Syst.*, vol. 16, no. 4, pp. 1806–1816, Aug. 2015.

[11] T. J. Wright, R. Agrawal, S. Samuel, Y. Wang, S. Zilberstein, and D. L. Fisher, "Effective cues for accelerating young drivers' time to transfer control following a period of conditional automation," *Accident Anal. Prevention*, vol. 116, pp. 14–20, Jul. 2018.

[12] T. Wada, K. Sonoda, T. Okasaka, and T. Saito, "Authority transfer method from automated to manual driving via haptic shared control," in *Proc. IEEE Int. Conf. Syst., Man, Cybern.*, 2016, pp. 2659–2664.

[13] M. Mulder, D. A. Abbink, and E. R. Boer, "Sharing control with haptics: Seamless driver support from manual to automatic control," *Human Factors*, vol. 54, no. 5, pp. 786–798, Oct. 2012.

[14] D. A. Abbink, M. Mulder, and E. R. Boer, "Haptic shared control: Smoothly shifting control authority ?," *Cogn. Technol. Work*, vol. 14, no. 1, pp. 19–28, Mar. 2012.

[15] R. Boink, M. M. van Paassen, M. Mulder, and D. A. Abbink, "Understanding and reducing conflicts between driver and haptic shared control," in *Proc. IEEE Int. Conf. Syst., Man, Cybern.*, 2014, pp. 1510–1515.

[16] C. Huang, C. Lv, F. Naghdy, and H. P. Du, "Reference-free approach for mitigating human-machine conflicts in shared control of automated vehicles," *IET Control Theory Appl.*, vol. 14, no. 18, pp. 2752–2763, Dec. 2020.

[17] T. Hiraoka, "How do we share the 'control" when using the haptic shared control for an advanced driver-assistance system?—Direct HSC and indirect HSC," *IFAC PapersOnLine*, vol. 52, no. 19, pp. 61–66, Sep. 2019.

[18] R. Li, S. Li, H. Gao, K. Li, and D. Li, "Effects of human adaptation and trust on shared control for driver-automation cooperative driving," Intell. Connected Veh. Symp., SAE Technical Paper 2017-01-1987, 2017, doi: 10.4271/2017-01-1987.

[19] M. Itoh and M. P. Pacaux-Lemoine, "Trust view from the human-machine cooperation framework," in *Proc. IEEE Int. Conf. Syst., Man, Cybern.*, 2018, pp. 3213–3218.

[20] J. Lee and N. Moray, "Trust, control strategies and allocation of function in human-machine systems," *Ergonomics*, vol. 35, no. 10, pp. 1243–1270, Oct. 2007.

[21] F. Wang, "Parallel control and management for intelligent transportation systems: Concepts, architectures, and applications," *IEEE Trans. Intell. Transp. Syst.*, vol. 11, no. 3, pp. 630–638, Sep. 2010.

[22] F. Wang, N. Zheng, D. Cao, C. M. Martinez, L. Li, and T. Liu, "Parallel driving in CPSS: A unified approach for transport automation and vehicle intelligence," *IEEE/CAA J. Autom. Sin.*, vol. 4, no. 4, pp. 577–587, Sep. 2017.

[23] V. A. Profillidis and G. N. Botzoris, *Modeling of Transport Demand*. Amsterdam, The Netherlands: Elsevier, 2019, pp. 163–224.

[24] C. Sentouh, P. Chevrel, F. Mars, and F. Claveau, "A sensorimotor driver model for steering control," in *Proc. IEEE Int. Conf. Syst., Man, Cybern.*, 2009, pp. 2462–2467.

[25] D. D. Salvucci and R. Gray, "A two-point visual control model of steering," *Perception*, vol. 33, no. 10, pp. 1233–1248, 2004.

[26] N. Tang, "The research of improved particle swarm optimization algorithm and its applications," M.S. thesis, Dept. Manage., Hefei Univ. Technol., Hefei, China, 2016.

[27] Y. Shi and R. C. Eberhart, "Parameter selection in particle swarm optimization," in *Proc. Int. Conf. Evol. Program.*, 1998, pp. 591–600.

[28] Y. Shi and R. Eberhart, "A modified particle swarm optimizer," in *Proc. IEEE World Congr. Comput. Intell.*, 1998, pp. 69–73.

[29] Y. Shi and R. C. Eberhart, "Empirical study of particle swarm optimization," in *Proc. Congr. Evol. Comput.*, 1999, pp. 1945–1950.

[30] F. Yu and Y. Lin, *Automobile System Dynamics*. Beijing, China: China Machine Press, 2005.

[31] Z. Yu, *Automobile Theory*. Beijing, China: China Machine Press, 2000.

[32] S. Zafeiropoulos and P. Tsiotras, "Design of a lane-tracking driver steering assist system and its interaction with a two-point visual driver model," in *Proc. Amer. Control Conf.*, 2014, pp. 3911–3917.

[33] M. Brown, J. Funke, S. Erlien, and J. C. Gerdes, "Safe driving envelopes for path tracking in autonomous vehicles," *Control Eng. Pract.*, vol. 61, pp. 307–316, 2017.

[34] X. Ji, K. Yang, X. Na, C. Lv, and Y. Liu, "Shared steering torque control for lane change assistance: A stochastic game-theoretic approach," *IEEE Trans. Ind. Electron.*, vol. 66, no. 4, pp. 3093–3105, Apr. 2019.